Available online at www.sciencedirect.com
ScienceDirect
Catalysis Today 128 (2007) 153–160
CATALYSIS TODAY
www.elsevier.com/locate/cattod

Catalytic and structural effects of W-substitution in M2 Mo-V-Te-oxide for propene ammoxidation

Johan Holmberg [a], Jakob B. Wagner [b], Robert Häggblad [a], Staffan Hansen [b], L. Reine Wallenberg [b], Arne Andersson [a,*]

[a] Department of Chemical Engineering, Lund University, Chemical Center, P.O. Box 124, SE-221 00 Lund, Sweden
[b] Division of Polymer and Materials Chemistry, Department of Chemistry, Lund University, Chemical Center, P.O. Box 124, SE-221 00 Lund, Sweden

Available online 9 August 2007

Abstract

Substitution of W for the Mo in M2-type Mo-V-Te-oxide was investigated. XRD, FTIR, XANES, and HRTEM verified that the substitution is possible in the whole range up to complete replacement of Mo by W. Catalytic measurements for propene ammoxidation show that both the specific activity and the selectivity to acrylonitrile pass through a maximum with increase of the W-content of the catalyst. XRD analysis indicates that the catalytic results, in part, can be explained by a disordered distribution of Mo, W, and V among the octahedral sites in M2 giving better catalytic performance than a more ordered arrangement does. Moreover, SEM and HRTEM imaging show that with increasing W-content, the M2 crystals change from μm-sized elongated crystals to spherical crystals of nm-size, influencing the type of surfaces being exposed and consequently the catalytic properties. Among the catalysts investigated, a catalyst with the composition $(Mo_{0.3}W_{0.7})_{1.9}V_{1.0}Te_{1.1}O_{10}$ is the most active and selective one, giving 80% selectivity to acrylonitrile.

Keywords: Ammoxidation; Propene; Acrylonitrile; Mo-V-W-Te-oxide catalysts; M2-phase; W-substitution; XRD; XANES; SEM; HRTEM

1. Introduction

The Mo-V-Nb-Te-oxide system is a promising catalyst system for oxidation and ammoxidation of propane to acrylic acid and acrylonitrile, respectively [1,2]. By now it is well established that this catalyst system consists of two orthorhombic phases, which are designated M1 and M2 (pseudo-hexagonal) [3–5]. In our previous work on the Mo-V-Nb-Te-oxide system for propane ammoxidation [6], we have shown that acrylonitrile is formed from propane via intermediate propene. Of the M1 and M2 phases, only M1 is active for converting propane to acrylonitrile, while both phases are active for converting propene to acrylonitrile. For the latter reaction, however, the M2 phase is more selective than M1 [7]. Therefore, tuning of the M2 phase is of interest not only as M2 together with M1 are components in propane (amm)oxidation catalysts, but also because M2 on its own rights being a candidate catalyst for propene ammoxidation. In the present work results are presented on the catalytic and structural effects of W-substitution for Mo in the M2 phase.

2. Experimental

Catalysts were prepared using the precursor method. The desired amounts of $(NH_4)_6Mo_7O_{24}{\cdot}4H_2O$, NH_4VO_3, H_6TeO_6, and $(NH_4)_6W_{12}(OH)_2O_{38}$ were dissolved together in water at 60 °C. Each batch consisted of metal salts corresponding to 5 g metals in 20 ml water. The water of the prepared solution was then allowed to evaporate in an oven equipped with forced air circulation, where the sample was kept for 4 h at 150 °C. The obtained precursor was then calcined in two steps in order to give the correct phase. In the first step, the precursor was calcined in air at 275 °C for 2 h and then in the subsequent step, for another 2 h under a flow of argon in a quartz reactor at 550 °C. The nominal composition of the preparations were $(Mo_{1-x}W_x)_{1.9}V_{1.0}Te_{1.1}O_{10}$ with x being varied from 0 to 1 (0, 0.3, 0.5, 0.7, and 1), which are denoted $Mo_{1-x}W_x$ for short in the text that follows.

* Corresponding author. Tel.: +46 46 2228280; fax: +46 46 149156.
E-mail address: Arne.Andersson@chemeng.lth.se (A. Andersson).

0920-5861/$ – see front matter © 2007 Elsevier B.V. All rights reserved.
doi:10.1016/j.cattod.2007.06.073

All catalysts were examined by X-ray powder diffraction (XRD) on a Seifert XRD 3000 TT diffractometer using Ni-filtered Cu Kα radiation. The instrument was calibrated using a silicon standard. The unit cell parameters were determined using the freeware PowderCell 2.4 written by W. Kraus and G. Nolze, Berlin. Crystal structure data was taken from Ref. [4] and the following parameters were varied in the Rietveld refinements: scale, specimen displacement and overall temperature factors, as well as lattice, background, peak width, and zero-point parameters, while the atomic positions were kept fixed. The effect of different degrees of ordering of the metal ions in the octahedra of the crystal structure of M2, was investigated using the PowderCell program. The occupancy factors for the relevant metal atoms were set at different values, and the experimental lattice parameters determined and the positional coordinates from Ref. [4] were utilized in the calculations.

FTIR-spectra were recorded on a Bruker IFS66 spectrometer. Measurements were performed in dry air on disks containing 3 mg of sample and 200 mg of KBr. The resolution was 4 cm^{-1} and 1000 scans were averaged.

The XANES measurements were performed at the I811 beamline at MAX-lab, Lund University. Spectra were recorded in transmission mode using three ionisation chambers. The sample was positioned between the first and second ionisation chamber, while a reference foil was positioned after the sample between the second and third ionisation chamber. XANES spectra were recorded for the V K-, Te L_3- and W L_3-edges using V, Ti, and Ga foils, respectively, as energy references. A Si(1 1 1) double crystal monochromator was used for the energy selection. For the measurements, the samples were ground and diluted with boron nitride to give an appropriate element concentration.

Scanning electron microscopy (SEM) images were acquired with a JEOL 6700F microscope. The acceleration voltage was set to 5 kV and the working distance to 8 mm. For high-resolution imaging (HRTEM), the samples were studied in a JEOL 3000F FEG transmission electron microscope operated at 300 kV and equipped with a CCD for image acquisition.

The specific surface areas of the catalysts were measured with a Micromeritics Flowsorb 2300 instrument using the single point BET method. Before measurement, the samples were degassed at 200 °C for 24 h.

The prepared catalysts were tested for ammoxidation of propene at atmospheric pressure and isothermal conditions using a plug-flow micro-reactor made of stainless steel. The catalyst load was 0.50–2.50 g, and the reactant flow of oxygen, ammonia, propene, and argon was varied between 10.2 and 23.1 N cm^3/min. The reaction temperature was set to 400 °C. To improve the temperature control of the reactor, it was embedded in an aluminium block and placed in a tube furnace. Propene, acrylonitrile, acetonitrile, acrolein, and CO_2 were analysed online using a gas chromatograph, which was equipped with an FID detector, a TCD detector and a Haysep Q column. The CO was analysed online with a Rosemount Binos 100 IR instrument.

3. Results

3.1. X-ray diffraction

The X-ray diffraction patterns in Fig. 1 of the prepared catalysts show that all samples are single phase, consisting of an orthorhombic (pseudo-hexagonal) M2-type of structure [4,5,7,8]. A comparison of the peak positions shows that replacement of Mo by W results in a shift of the peak positions, being due to the unit cell changes. The shift is best seen comparing the positions of the two peaks at ∼55°, which merge together when the W-content is increased. The refined lattice constants are displayed in Fig. 2 as a function of the degree of W-substitution. As can be seen, the lattice parameters of M2 vary linearly with the degree of substitution obeying Vegard's law. With increase of the W-content, the *a*- and *b*-axes increase while the *c*-axis shows the reverse variation, resulting in a small decrease of the unit cell volume.

Another trend seen in Fig. 1 is that on both sides of the strongest peak at 28° there are two strong peaks at 22 and 36°, respectively, whose intensity ratio depends on the degree of W-substitution. For Mo_1W_0, the former peak is the largest. With increase of the W-content, the latter becomes the largest. Model calculations confirmed that this change is in agreement with the replacement of Mo by W. Moreover, Mo_1W_0 and Mo_0W_1 show some very weak peaks at 24 and 27°, Mo_0W_1 also at 14°, confirming that although strongly pseudo-hexagonal, the structure is orthorhombic in agreement with previous detailed structure investigations [4,8]. The weak peaks belong to the M2-type phases, and the model calculations showed that the intensity of the peaks strongly increases with the degree of ordering of the metals as seen in Fig. 3, where the calculated diffraction patterns are given for the Mo_0W_1 composition with either complete disorder or order of the different metals. The corresponding diffraction patterns calculated for the Mo_1W_0 composition showed the same trend, although the corresponding peaks had

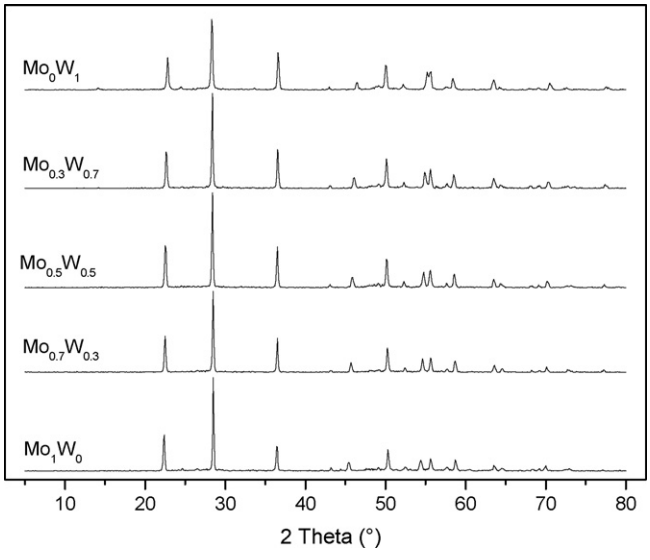

Fig. 1. XRD patterns of $(Mo_{1-x}W_x)_{1.9}V_{1.0}Te_{1.1}O_{10}$ samples with $x = 0.0$, 0.3, 0.5, 0.7, and 1.0.

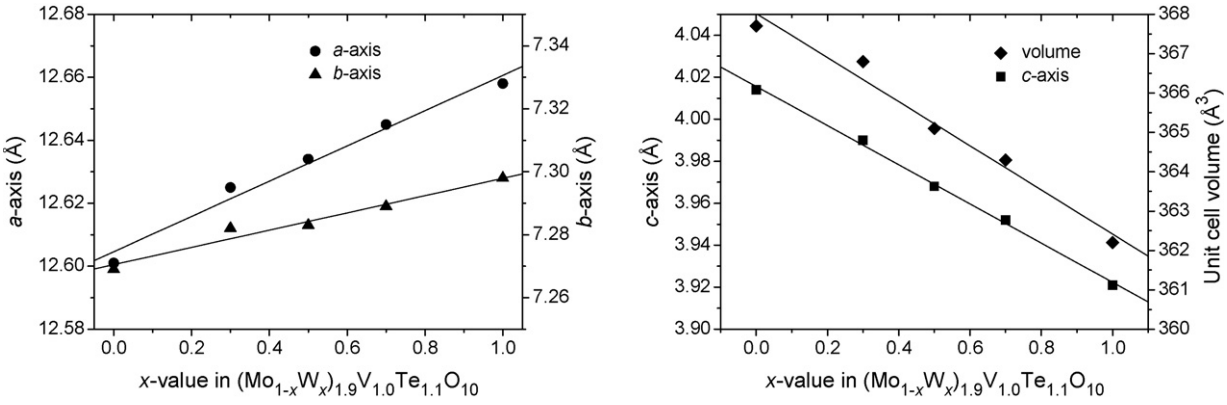

Fig. 2. Variation of the unit cell parameters as a function of the degree of W-substitution in $(Mo_{1-x}W_x)_{1.9}V_{1.0}Te_{1.1}O_{10}$.

slightly lower intensity. Comparing in Fig. 3 the calculated patterns with those recorded for $Mo_{0.5}W_{0.5}$ and Mo_0W_1, it is apparent that $Mo_{0.5}W_{0.5}$ is without order while Mo_0W_1 shows some ordering. Generally it was observed that the end compositions Mo_1W_0 and Mo_0W_1 are more ordered as compared to the samples with both Mo and W ($Mo_{0.7}W_{0.3}$, $Mo_{0.5}W_{0.5}$ and $Mo_{0.3}W_{0.7}$).

3.2. Infrared spectroscopy

In Fig. 4 are shown the IR spectra of the prepared catalysts. The spectrum of the unsubstituted Mo_1W_0 agrees with that previously being reported for the M2 phase [9]. Mo_1W_0 gives bands at 923, 854, 763, 733, 604, and 456 cm^{-1}. The IR spectra of the W-substituted samples are similar to that for Mo_1W_0. However, a few changes are observed. When the W-content is increased, the position of the band at 923 cm^{-1} (Mo_1W_0) shifts and appears at 945, 945, 941, and 929 cm^{-1}, respectively, for $Mo_{0.7}W_{0.3}$, $Mo_{0.5}W_{0.5}$, $Mo_{0.3}W_{0.7}$, and Mo_0W_1. Simultaneously, the wavenumber of the peak at 456 cm^{-1} (Mo_1W_0) gradually decreases to 429 cm^{-1} (Mo_0W_1). Moreover, in the spectra of the substituted samples a new band appears at ~835 cm^{-1}, the intensity of which increases with the W-content of the sample. It is also noticed that the ratio between

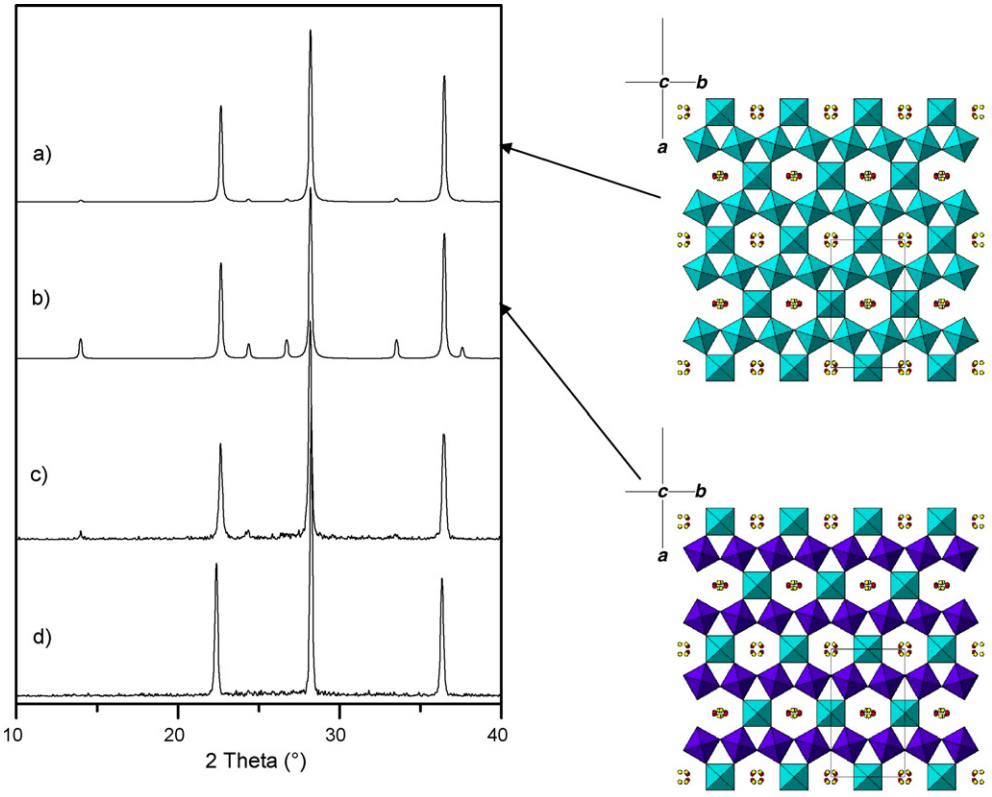

Fig. 3. A comparison of calculated and measured XRD patterns. (a) The XRD calculated for Mo_0W_1 with complete disorder of V and W; (b) the corresponding XRD assuming ordering of V and W; (c) the XRD measured for Mo_0W_1; (d) the XRD measured for $Mo_{0.5}W_{0.5}$. In the disordered structure the octahedra are randomly filled with 67% W or Mo and 33% V, the Te-sites are marked red and the oxygens linked to Te in the channels are marked yellow. In the ordered structure the violet octahedra are filled with W or Mo and the blue ones with V. Only one of the four symmetry related channel sites is occupied in each case, see Ref. [4].

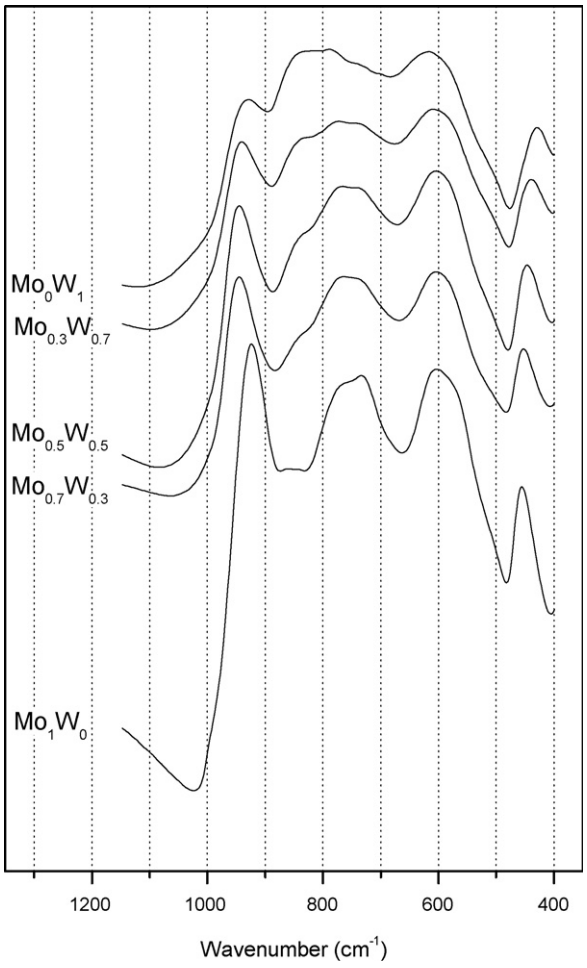

Fig. 4. Infrared absorbance spectra of prepared $(Mo_{1-x}W_x)_{1.9}V_{1.0}Te_{1.1}O_{10}$ catalysts.

the peak at ~900 cm^{-1} and the bands at 700–800 cm^{-1} decreases with increased W-content.

3.3. XANES

In order to determine the oxidation states of the metals in the M2-type structures, XANES spectra of the V K-, Te L_3- and W L_3-edges were recorded. No measurements could be performed on Mo due to experimental limitations. Fig. 5a shows the W L_3-edge spectra for $Mo_{0.5}W_{0.5}$, Mo_0W_1, and the reference compound WO_3. The spectra for the three samples, which show a strong white line, are almost identical with regard to both the edge position and the post-edge features.

V K-edge spectra are displayed in Fig. 5b for the unsubstituted Mo_1W_0 and the W-substituted $Mo_{0.5}W_{0.5}$ and Mo_0W_1 samples. For comparison, the corresponding spectrum for V_2O_5 is shown. All spectra show a pre-edge peak from the 1s → 3d transition [10]. For Mo_1W_0, $Mo_{0.5}W_{0.5}$, and Mo_0W_1, the pre-edge position is 5468.2 eV, and for V_2O_5 it is 5469.8 eV. There is a corresponding shift (~1.6 eV) of the main edge position.

Te L_3-edge spectra are given in Fig. 5c for Mo_1W_0, $Mo_{0.5}W_{0.5}$, and Mo_0W_1 together with those for the references TeO_2 and H_6TeO_6. All samples show a pre-edge peak around 4347 eV. In this case the position of the pre-edge peak is not discriminating of the oxidation state of Te as it is at 4346.7 eV for $Te(IV)O_2$ and the M2-type phases, while for $H_6Te(VI)O_6$ it is at 4346.9 eV. However, as seen in Fig. 5d, there is a ~2 eV difference in energy between the main edge positions of TeO_2 and H_6TeO_6. For Mo_1W_0, the main edge is positioned in-between those for TeO_2 and H_6TeO_6, and the same was observed for the samples with W.

3.4. Electron microscopy

The SEM micrographs in Fig. 6 show that the unsubstituted sample consists of agglomerated 0.5–1 μm large crystals (Fig. 6a), while W-substitution gives agglomerated crystals of reduced size. The $Mo_{0.5}W_{0.5}$ sample reveals agglomerated crystals of 100–500 nm in size (Fig. 6b), while the agglomerated crystals in sample Mo_0W_1 are smaller than 100 nm (Fig. 6c). The samples containing Mo reveal facets and have a preferred direction giving an elongated morphology, while the crystals of the fully W substituted sample has a more spherical shape.

HRTEM images show that the edges of the Mo_1W_0 catalyst are without any amorphous material (Fig. 7), although the structure and composition of the outmost layer may differ from that of the bulk.

3.5. Catalytic performance

The performances of the prepared catalysts were investigated for propene ammoxidation. In Fig. 8 are the specific reaction rates given together with the selectivities to acrylonitrile and acrolein at 30% propene conversion. Of other products mainly carbon oxides were produced with a minor amount of acetonitrile being formed with a selectivity of less than 2%. The Mo_1W_0 sample is active and gives both acrylonitrile and acrolein with selectivities of 52 and 27%, respectively. Compared with Mo_1W_0, the sample Mo_0W_1 without Mo is less active but more selective for acrylonitrile formation with a selectivity of 65% but, however, it gives no acrolein. For the samples with both Mo and W, the data shows that with increasing degree of W-substitution for Mo, both the activity and the selectivity to acrylonitrile increases in parallel with the selectivity to acrolein decreases. However, the total selectivity to the C_3-products acrylonitrile plus acrolein remains almost constant at about 80%. The most active sample is $Mo_{0.3}W_{0.7}$, which also is the best performing catalyst with a selectivity to acrylonitrile and acrolein of 80 and 3%, respectively.

4. Discussion

4.1. Structural aspects

The XRD results in Fig. 1 show that replacement by W of Mo in the Mo-V-Te-oxide M2 structure is possible in the whole range up to complete replacement. Moreover, the lack of any

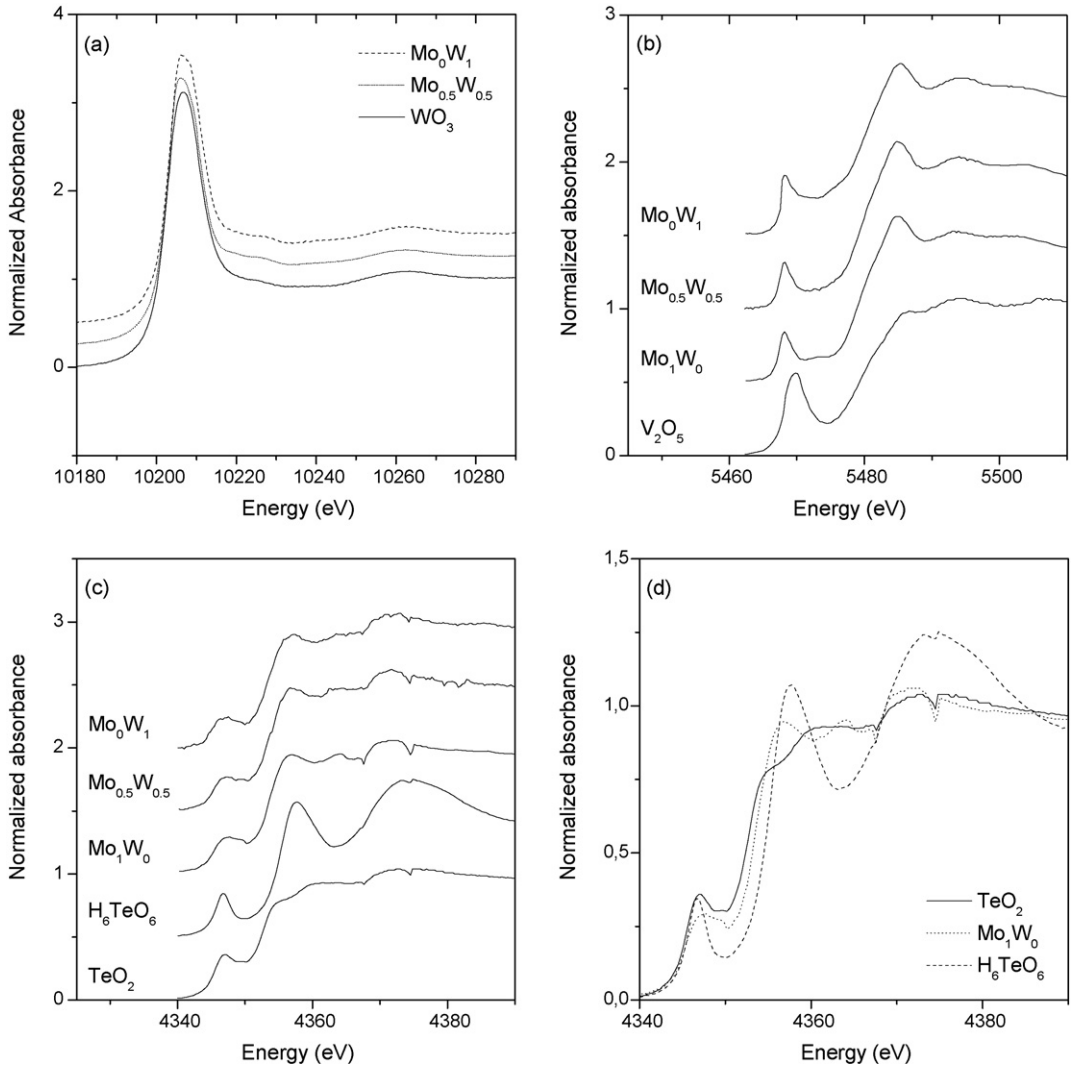

Fig. 5. Normalized W L_3-edge XANES spectra of WO_3, $Mo_{0.5}W_{0.5}$ and Mo_0W_1 (a), normalized V K-edge XANES spectra of V_2O_5, Mo_1W_0, $Mo_{0.5}W_{0.5}$, and Mo_0W_1 (b), and normalized Te L_3-edge XANES spectra of TeO_2, H_6TeO_6, Mo_1W_0, $Mo_{0.5}W_{0.5}$, and Mo_0W_1 (c). A comparison of the Te L_3-edge positions of TeO_2, H_6TeO_6, and Mo_1W_0 is shown in (d).

sign of the lattice parameters becoming constant (Fig. 2) or growing diffuse features in the background (Fig. 1) indicate that the formation of an XRD-amorphous bulk phase can be ruled out. In a previous investigation of the M1 and M2 phases, it was observed that the crystals were encapsulated with a 1–2 nm thick layer without long-range ordering and of different structure than the bulk material [11]. A similar surface texturing, however, was not observed by HRTEM imaging of our M2 samples. The image in Fig. 7 of the unsubstituted Mo_1W_0 shows that the bulk structure extends out to the edge, which is without any visible amorphous material. However, for the samples containing W, it was observed that a thin (1–2 nm) layer without any long-range ordering become more pronounced for higher W content in the sample. Furthermore, EDS measurements in the SEM shows the samples to be homogenous in composition. These observations, in combination with no other phases being observed, confirm that it is possible to completely replace Mo by W, which is in line with the ionic radius being almost the same for six-coordinated Mo^{6+} (0.73 Å) and W^{6+} (0.74 Å) [12]. That a relatively large amount of W can be accommodated in the M2 phase, moreover, is in agreement with the M2 structure being related to that of the bronzes (K, Rb, Cs)$_x$$W_3O_9$ where x being variable and has an upper limit of one [13]. The structure of M2, which is depicted in Fig. 3, is built of layers with corner sharing (Mo, V, W)O_6 octahedra forming three- and six-membered rings. The layers are connected by the octahedra sharing corners, giving hexagonal channels along the c-axis. In the bronzes the alkali metals are situated in the channels [13], and in M2 the channels are occupied by interconnected Te–O units forming chains along the c-axis [4,5,8].

The successful substitution of W for Mo is also consistent with the fact that the FTIR spectra of the catalysts in Fig. 4 show continuous spectral changes and shift in peak positions with increasing degree of substitution. Due to the fact that there are several metals in the structures, the bands are difficult to assign precisely. Therefore, the assignments made in the following have to be considered indicative only. Concerning the M1 and M2

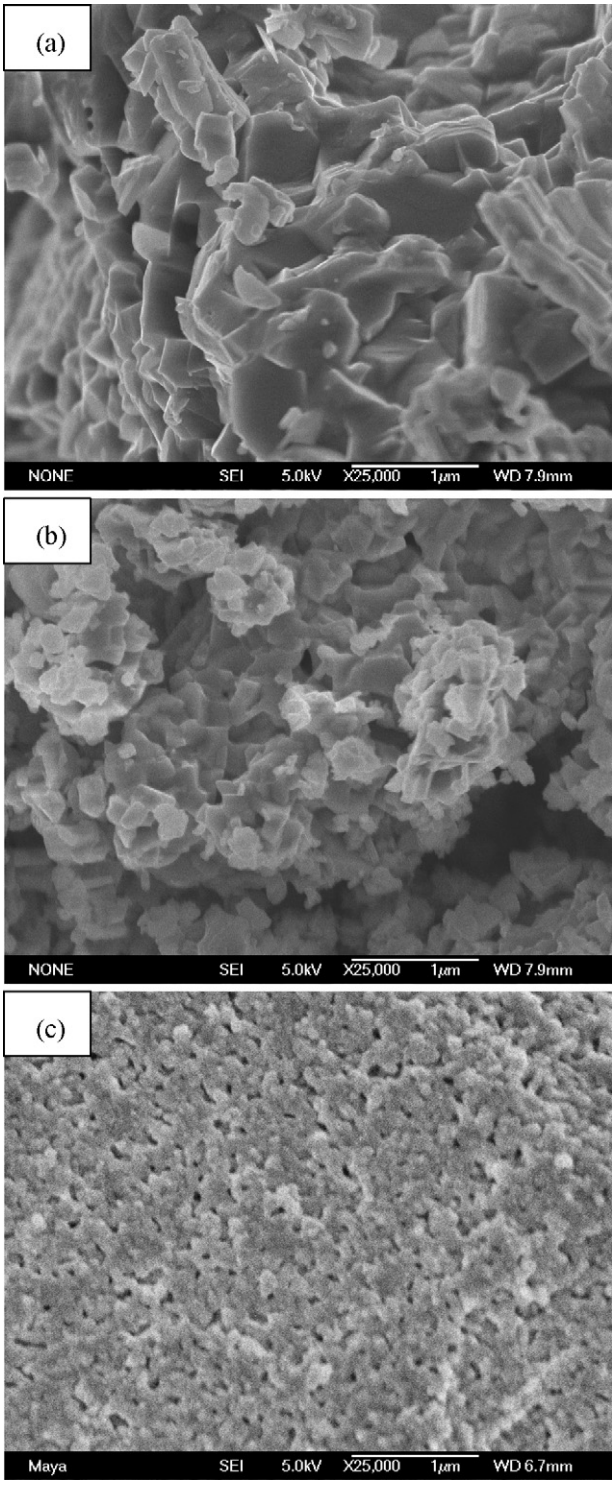

Fig. 6. SEM micrographs of the M2-type phases (a) Mo_1W_0, (b) $Mo_{0.5}W_{0.5}$, and (c) Mo_0W_1.

phases without W, bands in the region 1000–900 cm^{-1} have been assigned to Mo=O stretching vibrations, and bands at lower wavenumbers to Mo–O–M vibration modes where M = Mo, V, and Te [14]. Thus, considering the FTIR spectra in Fig. 4, the band at 923–945 cm^{-1} can be assigned to Mo=O, V=O, and W=O stretching modes, which typically give infrared bands in this region [15]. The fact that the intensity of this band relative to

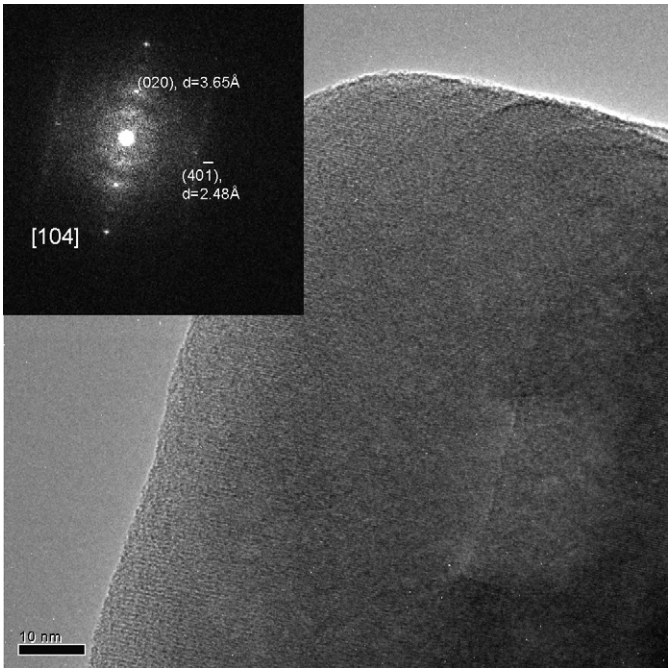

Fig. 7. High-resolution TEM showing a Mo_1W_0 crystal viewed along the [1 0 4] direction.

the 700–800 cm^{-1} region decreases with increase of the W-content and remains in the spectrum of Mo_0W_1 without Mo, indicates that it essentially is from Mo=O and V=O vibration modes. The band at 835 cm^{-1} can be assigned to a W–O–V vibration, considering that it is absent for Mo_1W_0 and the intensity of the band increases with the degree of W-substitution.

Regarding Te–O–M vibration modes, the band for Mo_1W_0 at 733 cm^{-1} can be assigned to a Te–O–Mo vibration [16] as the intensity of the band strongly decreases with increase of the W-content of the catalyst. A contribution from a Te–O–W mode cannot be excluded as the band is still seen in the spectrum of Mo_0W_1, although with much reduced intensity. It has been reported that the TeO_4 units in TeO_2 give an infrared band around 660 cm^{-1}, the exact position of which depends on the

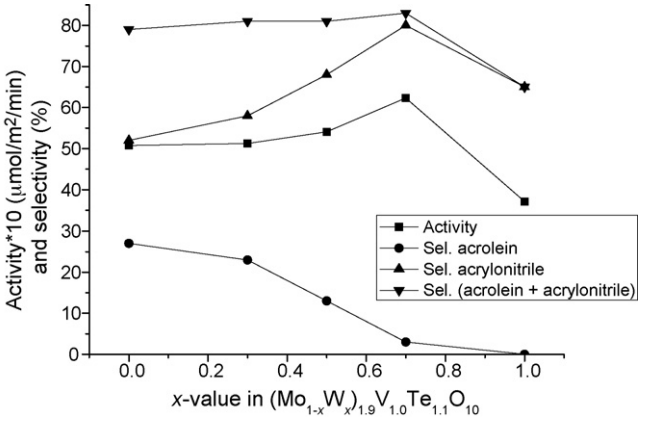

Fig. 8. Propene ammoxidation on $(Mo_{1-x}W_x)_{1.9}V_{1.0}Te_{1.1}O_{10}$. Reaction rates and selectivity data at 30% propene conversion are given for the formations of acrolein, acrylonitrile and the sum thereof. Reaction conditions: 400 °C, atmospheric pressure and the molar feed ratio propene:ammonia:oxygen:argon = 6.1:7.0:18.0:70.2.

Te–O distances [16]. When one of the oxygens is relatively distant to the metal, the peak shifts to 635 cm^{-1}. The peak shifts to even lower wavenumber (610 cm^{-1}) when the TeO_4 units are transformed into TeO_3 units through disruption of one of the Te–O bonds. Thus, the band shown by the catalysts at ~600 cm^{-1} can be assigned to a TeO_3 unit, which is in perfect agreement with the report [4] that some channels in M2 may contain distorted TeO_3E tetrahedra, with lone pair of electrons (E), as a result of weak interaction between the units along the *c*-direction. Crystalline $V_2O_5{\cdot}2TeO_2$ [17] and $MoO_3{\cdot}2TeO_2$ [16] both have infrared bands in the 400–500 cm^{-1} region. Considering it has been reported that the Te in the hexagonal channels in M2 are displaced towards V-sites [4], it seems reasonable to suggest that the band at 456 cm^{-1} in the spectrum of Mo_1W_0 is from a Te–O–V vibration. The observation that the band shifts towards lower wavenumbers upon substitution of W for Mo, indicates that the substitution affects the exact positioning of Te in the hexagonal channel.

In view of the stoichiometry of the unsubstituted ideal M2 being $(TeO)(Mo,V)_3O_9$ [4,5], it follows that all metals cannot be in their highest oxidation states. Bond valence calculations have indicated that the cations in M2 are Mo^{6+}, V^{4+}, and Te^{4+} [4]. However, this type of calculation is only indicative and not always conclusive. In this regard, XANES spectra allow more precise conclusions. The W L_3-edge XANES spectra in Fig. 5a conclusively show that W is present in the catalysts as octahedrally coordinated W^{6+}. For V, the V K-edge spectra in Fig. 5b show for the catalysts a shift of 1.6 eV towards lower energy compared to V_2O_5. A shift of this magnitude supports that the V is tetravalent in the catalysts, in agreement with the linear relationship that has been reported in the literature [18] to exist between the pre-peak position and the formal oxidation state of V. The Te L_3-edge spectra of the catalysts in Fig. 5c are almost identical irrespective of the W-content. As shown in Fig. 5d, the main edge position falls in-between those for Te in TeO_2 and H_6TeO_6. The Te in TeO_2 is tetravalent with trigonal bipyramidal coordination TeO_4E with a lone pair of electrons (E), while the Te in H_6TeO_6 is hexavalent with octahedral coordination TeO_6. Considering both the position of the main edge and the post-edge features for the catalyst samples, it can be suggested that Te is present both as Te^{4+} and Te^{6+} in the M2-type catalysts. The observation of tetravalent Te is in agreement with the previous EXAFS study [5], where it was concluded that the hexagonal channels in M2 are occupied by trigonal bipyramidal TeO_4E entities, which are bonded together via oxygen forming infinite chains along [0 0 1]. The indication that the catalysts may contain also some Te^{6+} in octahedral coordination is in line with the compositions of the catalysts being $(Mo_{1-x}W_x)_{1.9}V_{1.0}Te_{1.1}O_{10}$ with 10% Te in excess of the amount that is required for filling up the hexagonal channels. The excess Te can be hexavalent and occupy some of the octahedral sites in agreement with the formula $(Mo_{1-x}W_xTe_{0.05})_{1.9}V_{1.0}Te_{1.0}O_{10}$. This assumption is supported by the fact that six-coordinated Te^{6+}, Mo^{6+}, and W^{6+} have similar ionic radii, which are 0.70, 0.73, and 0.74 Å, respectively [12]. As W is hexavalent in the catalysts, and the oxidation states of V and Te are independent of the degree of replacement of Mo by W, it follows from the stoichiometry that Mo is hexavalent in the M2-type phases.

4.2. Catalytic aspects

Fig. 8 shows that both the catalytic activity and the selectivity to acrylonitrile increase with increasing degree of substitution up to 70% replacement ($Mo_{0.3}W_{0.7}$) by W of the Mo in the M2-type phase. It is moreover seen that the increase of the selectivity to acrylonitrile is due to less acrolein being formed, indicating more efficient ammonia activation as a result of introduction in the structure of W, which is more acidic than Mo. This result has some similarity with the performance of the Al-Sb-V-W-oxide system for propane ammoxidation, where it was observed that the addition of W gives higher activity and more selective activation of ammonia, resulting in higher yield to the formation of acrylonitrile [19]. The present results can be interpreted as a V-site rather than a Mo-site being involved in the activation of propene. However, we have previously demonstrated that replacement of up to 50% of the V by Ti gives a 60% increase of the activity without affecting the selectivity [20]. Therefore, it seems reasonable to anticipate that both Mo–O–Te and V–O–Te sites are active and selective. However, the replacement of Mo by W increases the number of W–O–V connections at the expense of Mo–O–V connections. Obviously, as the Mo–O–V configuration gives more acrolein, it seems to be less effective for the appropriate activation of ammonia and the subsequent insertion of an –NH species into the allylic intermediate formed from propene [21]. Generally it is considered that a Te^{4+} site with a lone pair of electrons is performing the first hydrogen abstraction from propene being adsorbed on a neighbouring cation [21,22]. Concerning the effect of W-substitution on the activity, this can be caused by structural means in agreement with the infrared data indicating an effect of W-substitution on the V–O–Te vibration mode at ~450 cm^{-1}.

However, the reasoning above cannot fully explain the fact that Mo_0W_1 is less active than Mo_1W_0 and, moreover, less selective than $Mo_{0.3}W_{0.7}$ to acrylonitrile formation. Therefore, also other factors have to be considered. One of these factors is disorder. In this respect, the XRD data and analysis presented in Fig. 3 show that the arrangement of the different cations in Mo_0W_1 and Mo_1W_0 is more ordered than in the samples containing both Mo and W. Thus, it seems that a disordered distribution among the octahedral sites of the different cations gives improved catalytic performance as compared to a more ordered arrangement. Another factor to consider is the type of exposed crystal surfaces. With increasing degree of W-substitution, SEM imaging reveals a change from well facetted μm-sized crystals to nm-sized crystals of more spherical shape (see Fig. 6). Consequently, there is an associated change of the type of exposed surfaces, a fact that should influence the catalytic performance. Moreover, as the drawings of the M2 structures in Fig. 3 show, different types of surface planes have different geometrical arrangement and may also have different ratio between channel and octahedral sites. A surface in a specific direction also can terminate differently, e.g. the surface perpendicular to the *a*-direction can expose either octahedral sites only, or

both octahedral and channel sites in the 1:1 ratio. Although no amorphous surface structure was observed in HRTEM (see Fig. 7), the termination and the composition of the very first layer cannot be determined. Our previous XPS analysis, however, indicated that the surfaces are richer than the bulk in Te [20].

5. Conclusions

Our results show that substitution of W for Mo is possible up to complete substitution retaining the orthorhombic pseudo-hexagonal M2-type structure. In the phases with both Mo and W, the distribution of the metals among the octahedral positions is more disordered compared to when only one of Mo and W is present.

XANES spectra show that in $(Mo_{1-x}W_x)_{1.9}V_{1.0}Te_{1.1}O_{10}$, W and Mo are hexavalent and V is tetravalent. The Te L_3-edge spectra indicate two types of Te in the structure, namely Te^{4+} in hexagonal channels and some Te^{6+} in octahedral positions.

SEM and TEM images demonstrate that with increasing W-content, the crystal size of the M2-type phase decreases from μm to nm size. In parallel the morphology of the crystals changes and consequently, the type of surfaces being exposed.

The activity and the selectivity to acrylonitrile pass through a maximum with increase of the W-content. These dependences can be explained by a disordered distribution of Mo, V, and W in the octahedral sites creating spatially isolated ensembles on the nano-scale with better catalytic performance as compared to structures with a more ordered arrangement of the cations. Moreover, the influence from the crystal size on the morphology and the distribution of the crystal faces being exposed affects the catalytic properties. A catalyst with the composition $(Mo_{0.3}W_{0.7})_{1.9}V_{1.0}Te_{1.1}O_{10}$ is the best performing with a selectivity to acrylonitrile of 80%.

Acknowledgements

J. Holmberg, R. Häggblad, A. Andersson, J.B. Wagner and L.R. Wallenberg acknowledge financial support from the Swedish Research Council. We are also grateful for the support received through the EU-funded Coordination Action of Nanostructured Catalytic Oxide Research and Development in Europe (CONCORDE).

References

[1] T. Ushikubo, H. Nakamura, Y. Koyasu, S. Wajiki, US Patent 5,380,933 to Mitsubishi Kasei Corporation (1995).
[2] T. Ushikubo, K. Oshima, A. Kayo, T. Umezawa, K. Kiyono, I. Sawaki, European Patent 529,853 to Mitsubishi Kasei Corporation (1996).
[3] T. Ushikubo, K. Oshima, A. Kayou, M. Hatano, in: C. Li, Q. Xin (Eds.), Stud. Surf. Sci. Catal., 112, Elsevier, Amsterdam, 1997, pp. 473–480.
[4] P. DeSanto Jr., D.J. Buttrey, R.K. Grasselli, C.G. Lugmair, A.F. Volpe Jr., B.H. Toby, T. Vogt, Z. Kristallogr. 219 (2004) 152.
[5] J.M.M. Millet, H. Roussel, A. Pigamo, J.L. Dubois, J.C. Jumas, Appl. Catal. A 232 (2002) 77.
[6] J. Holmberg, R.K. Grasselli, A. Andersson, Top. Catal. 23 (2003) 55.
[7] J. Holmberg, R.K. Grasselli, A. Andersson, Appl. Catal. A 270 (2004) 121.
[8] E. Garcia-González, J.M. López Nieto, P. Botella, J.M. González-Calbet, Chem. Mater. 14 (2002) 4416.
[9] P. Botella, J.M. López Nieto, B. Solsona, Catal. Lett. 78 (2002) 383.
[10] B. Moraweck, in: B. Imelik, J.C. Vedrine (Eds.), Catalyst Characterization—Physical Techniques for Solid Materials, Plenum Press, New York, 1994, pp. 377–416.
[11] J.B. Wagner, O. Timpe, F.A. Hamid, A. Trunschke, U. Wild, D.S. Su, R.K. Widi, S.B. Abd Hamid, R. Schlögl, Top. Catal. 38 (2006) 51.
[12] R.D. Shannon, Acta Crystallogr. Sect. A32 (1976) 751.
[13] A. Magnéli, Acta Chem. Scand. 7 (1953) 315.
[14] J.M. López Nieto, P. Botella, B. Solsona, J.M. Oliver, Catal. Today 81 (2003) 87.
[15] W.P. Griffith, P.J.B. Lesniak, J. Chem. Soc. A (1969) 1066.
[16] Y. Dimitriev, J.C.J. Bart, V. Dimitrov, M. Arnaudov, Z. Anorg. Allg. Chem. 479 (1981) 229.
[17] J. Dimitriev, M. Arnaudov, V. Dimitrov, Monatsh. Chem. 107 (1976) 1335.
[18] M. Baca, J.M. Millet, Appl. Catal. A 279 (2005) 67.
[19] J. Nilsson, A.R. Landa-Cánovas, S. Hansen, A. Andersson, J. Catal. 186 (1999) 442.
[20] J. Holmberg, S. Hansen, R.K. Grasselli, A. Andersson, Top. Catal. 38 (2006) 17.
[21] R.K. Grasselli, J.D. Burrington, D.J. Buttrey, P. DeSanto Jr., C.G. Lugmair, A.F. Volpe Jr., T. Weingand, Top. Catal. 23 (2003) 5.
[22] R.K. Grasselli, G. Centi, F. Trifirò, Appl. Catal. 57 (1990) 149.